International Journal of Scientific Research and Engineering Development-– Volume 3 - Issue 5, Sep - Oct 2020

Available at www.ijsred.com

RESEARCH ARTICLE OPEN ACCESS

Influence of Reservoir Variables on the Onset of Thermosolutal Convection in the Niger Delta

Onengiyeofori A. Davies*[1], Chigozie Israel-Cookey[1], Etim D. Uko[1], Mathew A. Alabraba [1]

[1] Physics Department, River State University, Port Harcourt, Rivers State, Nigeria

* davies.onengiyeofori@ust.edu.ng

----------**********----------

Abstract:

Capturing and storing anthropogenic carbon dioxide (CO_2) in deep geologic reservoirs promises to be a potential solution in the fight against drastic climatic change as a result of global warming driven by the presence of excess greenhouse gases (CO_2 inclusive) in our atmosphere. The convective dissolution of the sequestered CO_2 in the ambient brine is known to be one of the mechanisms in place to trap the sequestered CO_2. This study is aimed at investigating reservoir parameters that could serve to influence convective mixing post sequestration. To do this, linear stability analysis, relative to a set of hydrodynamic governing equations for a heterogeneous media where thermal and solutal fields contributed to the buoyant field in opposing manner, was carried out. Variables like permeability anisotropy ratio, porosity, Prandtl number and solutal Rayleigh number were investigated within this study relative to the onset of convective instability as defined by a 2D plot of thermal Rayleigh number and perturbation wave number. Results showed that convective instability, convective mixing in essence, was hastened by increasing anisotropy ratio, porosity and Prandtl, while an increasing solutal Rayleigh number delayed the onset of convective instability, thereby delaying convective mixing.

Keywords **—Thermosolutal Convection, Permeability Anisotropy Ratio, Porosity, Rayleigh Number, Prandtl Number.**

----------**********----------

I. INTRODUCTION

One proffered solution to the problem of accumulation of anthropogenic CO_2 in the earth's atmosphere is capture and storage of the said CO_2, by injecting the captured CO_2 into deep, about $2{,}600ft$ to $10{,}000ft$[1], geological reservoirs for safe keeping. This willessentially minimize the risk of leakage of the sequestered CO_2 back into the atmosphere. One of the mechanisms in place to trap the buoyant CO_2, injected in a supercritical phase, is its dissolution into the ambient brine of the geological reservoir through *convective dissolution*, a process that increases the rate of dissolution of the sequestered CO_2 in the ambient brine [2, 3]

When injected, the less dense supercritical CO_2, being relatively 'lighter', floats on top of the ambient brine under the influence of gravity. Across the interface between ambient brine and sequestered CO_2, which is flat at thermodynamic equilibrium [4], the weakly soluble CO_2 gradually dissolves in the ambient brine, producing a stratum of denser CO_2-rich brine between sequestered CO_2 and ambient brine. This will eventually give rise to the formation of buoyancy-driven convective instabilities with increase in the concentration of dissolved CO_2, causing the CO_2-rich brine to sink towards the bottom of the reservoir while sweeping fresh ambient brine to the top of the reservoir.

The involvement of temperature and concentration in influencing the buoyancy of a fluid is known as *thermosolutal* convection, a process often referred to as double-diffusive convection [5, 6]. According to Pritchard and Richardson [5], the most fascinating dynamics of this kind of convection is when the buoyancy field is influenced in opposite directions by the thermal and solutal fields, i.e. as one act to boost the buoyancy field the other will be acting to hinder it. Substantial reviews have been carried out by different authors relative to double-diffusive convection in porous media.

Looking to predict storage capacities, dissolution rate and time-scales relative to CO_2 convective dissolution, various theoretical and experimental studies have been carried out [7]. Theoretically, the convective dissolution of sequestered CO_2 is studied by modelling the storage reservoir as a two-dimensional idealized porous medium containing two-layering of pure CO_2 and brine [8, 9, 10]

Horton and Rogers Jr [11] and Lapwood [12] have been credited as the first set of independent researchers on the issue of density-driven convective dissolution within a body of fluid to a conclusion that $4\pi^2$ is the critical value of thermal Rayleigh number at which convection is initiated

Quite recently, in their experimental studies, Farajzadeh et al. [13] investigated how natural convection influences the sequestered CO_2 in a dual layer, anisotropic sub-surface porous formation saturated with water. They showed that the onset of natural convection is fastest for large permeability anisotropy ratios. They also showed that the flow is dominated

by natural convection when a highly permeable layer overlays the aquifer.

Hirata et al. [14] investigated the onset of double-diffusive (thermosolutal) natural convection in a horizontal superposed fluid and porous layers. Carrying out linear stability analysis, they showed that when thermosolutal convection is initiated in the porous media, the fluid region is characterized by a multi-cellular flow for negative thermal Rayleigh number while convective flows are initiated in both fluid and porous regions for positive Rayleigh numbers.

Li [15], in investigating fluid transport during different CO_2 transport trappings in saline aquifers, proposed a novel reactive diffusion-convection transport model. He showed that rates of reaction and diffusion had notable effects on the dynamics of the diffusion-convection-reaction of the CO_2-brine system.

Bhadauria [6], intending to describe the onset criteria for stationary and oscillatory double-diffusive convections, investigated double-diffusive convection with internal heating source, with the thermal and solutal source from below, in an anisotropic porous layer. By carrying out linear and non-linear stability analysis, they showed that the rates of heat and solute transfer increased with increasing internal Rayleigh number and anisotropy parameter while solute transfer decreased with increasing solutal Rayleigh number and Vadesz number, with the rate of solute transfer greater than the rate of heat transfer.

Akand et al. [16] carried out a numerical analysis to investigate the onset of thermosolutal convection of CO_2 in a two-dimensional brine saturated porous media. Their main focus being the influence of solutal and thermal buoyancy on the spread of convection front, they concluded that convection is better enhanced for laterally continuous geothermal reservoir relative to a deeper one.

By modelling and simulating the solubility trapping structure of CO_2 sequestration, Negara et al. [17] investigated the transport of sequestered CO_2 in an anisotropic porous media, including the dissolution-diffusion-convection processes. They showed that the increase in density of the formation fluid as a result of dissolved CO_2 has a linear relationship with the onset of convection, the CO_2 mass flux and the total dissolved mass.

De Paoli et al. [18] investigated the influence of anisotropic permeability on convection in porous media through direct numerical simulation of the distribution of the solutal concentration. By examining evolution of time of solutal dynamics, they concluded that the short-term amount of CO_2 that can be diffused in an anisotropic sedimentary rock is much larger relative to an isotropic sedimentary rock.

In investigating the effects of Soret and magnetic field on double-diffusive convection in porous media with concentration based internal heat source, Israel-Cookey et al. [19] employed linear stability analysis to determine the onset of convection. They were able to show that increasing Soret number quickened the onset of convection while increasing the Hartmann number (the magnet field parameter) delayed the onset of convection.

Most of these studies suggest that the dynamics of such a system can be characterized by the Rayleigh number, Ra, which is a dimensionless number that aids in predicting natural convection [20]. Quite often, there is usually a critical threshold for the associated Rayleigh number, Ra_c, above which there would be an onset of convective instability [21, 22].

One way to further characterize the onset of convective dissolution in any system of interest is through linear stability analysis to estimate neutral stability curves, with the minimum of such curves defining the critical time at which convective instability is brought about [23].

II. THE GEOTHERMAL RESERVOIR MODEL

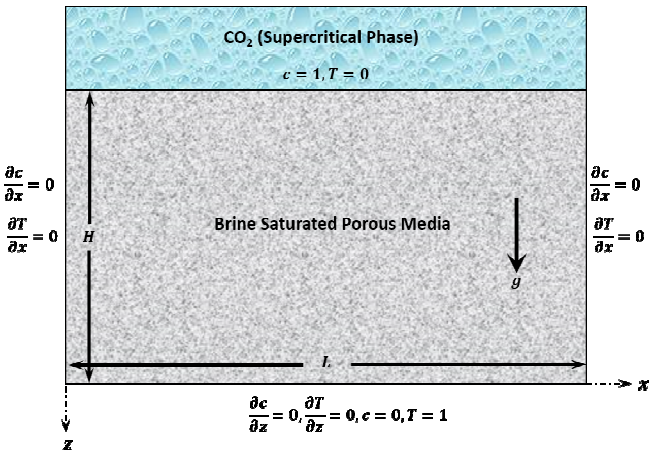

Fig. 1:Schematic for Geothermal Reservoir Model

Figure 1 is a schematic of the reservoir model that will be analysed in this work to characterize the onset of instability in the event of carbon sequestration in a typical Niger Delta reservoir rock. For this purpose, the model is considered to be a 2-dimensional reservoir that is saturated to a height H and length L with brine.

This model is such that there is a spatial variability of its permeability, i.e. $k = k(x, z)$, since the reservoirs in the Niger Delta region have been described by many authors as being anisotropic [24, 25]. To reduce complexities in the mathematical process, it would be assumed that there is no solute and heat fluxes across lateral boundaries (this is however not necessarily true, geologically, as there could still be low rate flux diffusion into the low-permeability bounding surfaces. The top and bottom boundaries will be assumed to be isothermally cold and hot respectively, with pressure changes due to dissolution across the CO_2-brine interface not accounted for as this interface is assumed to be sharp. Additionally, it would also be assumed that, before dissolution begins, the reservoir contains a single fluid phase. Geochemical reaction processes would be ignored, as it will be assumed that velocity-based capillary and dispersion effects are negligible. The boundary conditions will be opposite for concentration and temperature, as it will be

assumed that the reservoir is heated from bottom and thus the temperature at the bottom of the modelled reservoir will be higher than the temperature at its top. This boundary conditions will be such that at $z = 0$, $C = 1$ and $T = 0$, while at $z = H$, $C = 0$ and $T = 1$. Natural convection will then be driven by density gradient as a result of variation in solute concentration and temperature**.**

It is important to note that these assumptions are valid for geothermal reservoirs deeper than 3,280 ft [26]. Therefore, the governing equations relative to fields of concentration and flow of this model will be Darcy's law (in the x- and z-directions), continuity equation for incompressible fluid, convection-diffusion equation and the energy equation [16, 27, 28]**.**

$$v_x = -\frac{k_x}{\mu}\frac{\partial P}{\partial x} \quad (1)$$

$$v_z = -\frac{k_z}{\mu}\left[\frac{\partial P}{\partial z} - \rho g\right] \quad (2)$$

$$\frac{\partial v_x}{\partial x} + \frac{\partial v_z}{\partial z} = 0 \quad (3)$$

$$\frac{\phi \partial C}{\partial t} + v_x\frac{\partial C}{\partial x} + v_z\frac{\partial C}{\partial z} = \phi D\left[\frac{\partial^2 C}{\partial x^2} + \frac{\partial^2 C}{\partial z^2}\right] \quad (4)$$

$$\rho_o C_p\left[\frac{\partial T}{\partial t} + v_x\frac{\partial T}{\partial x} + v_z\frac{\partial T}{\partial z}\right] = \kappa\left[\frac{\partial^2 T}{\partial x^2} + \frac{\partial^2 T}{\partial z^2}\right] \quad (5)$$

Where;

$v_x =$ Component of fluid velocity in the x-direction (ms^{-1})

$v_z =$ Component of fluid velocity in the z-direction (ms^{-1})

$P =$ Pressure (Pa)

$\rho =$ Fluid density (kgm^{-3})

$k_x =$ Component of permeability in the x-direction (m^2)

$k_z =$ Component of permeability in the z-direction (m^2)

$\mu =$ Viscosity $(kgm^{-1}s^{-1})$

$g =$ Acceleration due to gravity (ms^{-2})

$\phi =$ Porosity

$C =$ Solute concentration

$D =$ Diffusion Coefficient (m^2s^{-1})

$C_p =$ Heat capacity at constant pressure $(Jkg^{-1}K^{-1})$

$T =$ Solute temperature (K)

$\kappa =$ Thermal conductivity $(Wm^{-1}K^{-1})$

According to Akand et al. [27], since a small change in density within the fluid is relative to temperature and concentration alterations at constant pressure, density of brine (ρ) within the fluid system of interest can be assumed to be linearly dependent on temperature (T) and solute concentration (C) in such a way that;

$$\rho = \rho_o[1 + \beta_C(C - C_o) - \beta_T(T - T_o)] \quad (6)$$

Where $\beta_C = \frac{1}{\rho_o}\left(\frac{\partial \rho}{\partial C}\right)$ and $\beta_T = -\frac{1}{\rho_o}\left(\frac{\partial \rho}{\partial T}\right)$ are coefficient of density increase by concentration and coefficient of thermalexpansion respectively. Evidently, the coefficients β_C and β_T could either be positive or negative: with a positive sign indicative of a destabilizing effect and negative sign indicative of a stabilizing effect [5]. Therefore, the dynamics here presented is a case of opposing effects of thermal and solute fields on the total buoyancy field, with the solutal field acting to destabilize while the thermal field is stabilizing. This will result in a scenario where instability is initiated in the motionless conductive state, with increasing Rayleigh number (solutal or thermal), through a supercritical bifurcation to a state of steady convective motion with a finite amplitude [5].

Differentiating equation *6*with respect to x;

$$\frac{\partial \rho}{\partial x} = \rho_o\left[\beta_C\frac{\partial C}{\partial x} - \beta_T\frac{\partial T}{\partial x}\right] \quad (7)$$

To eliminate the pressure term in our set of governing equations, cross differentiating equations *1* and *2*and finding their difference;

$$\frac{1}{k_Z}\frac{\partial v_z}{\partial x} - \frac{1}{k_x}\frac{\partial v_x}{\partial z} = \frac{g}{\mu}\frac{\partial \rho}{\partial x} \quad (8)$$

Inserting equation *7*into *8***;**

$$\frac{1}{k_Z}\frac{\partial v_z}{\partial x} - \frac{1}{k_x}\frac{\partial v_x}{\partial z} = \frac{g\rho_o}{\mu}\left[\beta_C\frac{\partial C}{\partial x} - \beta_T\frac{\partial T}{\partial x}\right] \quad (9)$$

Since the model applied here involves a two-dimensional mass flux, the mass flux vector, ρV, can be represented by a *scalar stream function* denoted by $\psi(x, z)$, which Rylov [29] defined as an arbitrary function whose partial derivative in any direction describes the velocity in that direction, helping to describe the velocity characteristics of the streamline of flow thought out the flow domain. Mathematically;

$$v_x = -\frac{\partial \psi}{\partial z} \quad (10)$$

$$v_z = \frac{\partial \psi}{\partial x} \quad (11)$$

With these new mathematical formulations in mind, the sets of governing equations that would be applied to the model of interest include;

$$\frac{1}{k_z}\frac{\partial^2 \psi}{\partial x^2} + \frac{1}{k_x}\frac{\partial^2 \psi}{\partial z^2} = \frac{g\rho_o}{\mu}\left[\beta_C\frac{\partial C}{\partial x} - \beta_T\frac{\partial T}{\partial x}\right] \quad (12)$$

$$\frac{\phi \partial C}{\partial t} - \frac{\partial \psi}{\partial z}\frac{\partial C}{\partial x} + \frac{\partial \psi}{\partial x}\frac{\partial C}{\partial z} = \phi D\left[\frac{\partial^2 C}{\partial x^2} + \frac{\partial^2 C}{\partial z^2}\right] \quad (13)$$

$$\frac{\partial T}{\partial t} - \frac{\partial \psi}{\partial z}\frac{\partial T}{\partial x} + \frac{\partial \psi}{\partial x}\frac{\partial T}{\partial z} = \frac{\kappa}{\rho_o C_p}\left[\frac{\partial^2 T}{\partial x^2} + \frac{\partial^2 T}{\partial z^2}\right] \quad (14)$$

Equations *12, 13*and *13* are then to be solved to obtain expressions for ψ, C and T.

A. Non-Dimensionalisation of Governing Equations

According to Ennis-King et al. [26] and Akand et al. [16], considering the height of the model reservoir (H), these dimensionless variables (bold characters) will be applied to aid in the non-dimensionalisation of the governing equations;

$$\boldsymbol{x} = \frac{x}{H}, \qquad \boldsymbol{z} = \frac{z}{H}, \qquad \boldsymbol{\psi} = \frac{\psi}{\phi \mathrm{D}}, \qquad \boldsymbol{t} = \frac{D}{\mathrm{H}^2}t,$$

$$\boldsymbol{C} = \frac{C - C_r}{\mathrm{C_o} - C_r} \& \qquad \boldsymbol{T} = \frac{T - T_r}{\mathrm{T_o} - T_r}$$

Where the 'r' and 'o' subscripts are indicative of reference and base state variables respectively. Inserting these into equations *12*, *13* and *14*, and accounting for the effect of anisotropy and defining a permeability anisotropy ratio $\vartheta = \frac{k_z}{k_x}$,

$$\frac{\partial^2 \boldsymbol{\psi}}{\partial \boldsymbol{x}^2} + \vartheta \frac{\partial^2 \boldsymbol{\psi}}{\partial \boldsymbol{z}^2} = Ra_S \frac{\partial \boldsymbol{C}}{\partial \boldsymbol{x}} - Ra_T \frac{\partial \boldsymbol{T}}{\partial \boldsymbol{z}} \tag{15}$$

$$\frac{\partial \boldsymbol{C}}{\partial \boldsymbol{t}} - \frac{\partial \boldsymbol{\psi}}{\partial \boldsymbol{z}}\frac{\partial \boldsymbol{C}}{\partial \boldsymbol{x}} + \frac{\partial \boldsymbol{\psi}}{\partial \boldsymbol{x}}\frac{\partial \boldsymbol{C}}{\partial \boldsymbol{z}} = \frac{\partial^2 \boldsymbol{C}}{\partial \boldsymbol{x}^2} + \frac{\partial^2 \boldsymbol{C}}{\partial \boldsymbol{z}^2} \tag{16}$$

$$\frac{\partial \boldsymbol{T}}{\partial \boldsymbol{t}} - \phi \frac{\partial \boldsymbol{\psi}}{\partial \boldsymbol{z}}\frac{\partial \boldsymbol{T}}{\partial \boldsymbol{x}} + \phi \frac{\partial \boldsymbol{\psi}}{\partial \boldsymbol{x}}\frac{\partial \boldsymbol{T}}{\partial \boldsymbol{z}} = \frac{1}{Pr}\left[\frac{\partial^2 \boldsymbol{T}}{\partial \boldsymbol{x}^2} + \frac{\partial^2 T}{\partial \boldsymbol{z}^2}\right] \tag{17}$$

Equations *15*, *16* and *17* are non-dimensional form of the governing equations. Where;

$Ra_S =$ Solutal Rayleigh number $= \frac{k_z \rho_o H g \beta_C \Delta C}{\mu \phi D} = \frac{k_z H g \Delta \rho_C}{\mu \phi D}$

$Ra_T =$ Thermal Rayleigh number $= \frac{k_z \rho_o H g \beta_T \Delta T}{\mu \phi D} = \frac{k_z H g \Delta \rho_T}{\mu \phi D}$

$Pr =$ Prandtl Number $= \frac{\rho_o C_p D}{\kappa}$

B. Linear Stability Analysis

Linear stability analysis will be carried out relative to the non-dimensional governing equations to quantitatively describe the onset of convective instability in the reservoir of interest. This will aid in investigating the growth or evolution of the disturbance within the system, due to density differential, relative to time, by defining a critical Rayleigh number above which buoyancy-driven convection will be initiated.

First and foremost, a steady state solution will be sought after to determine whether the governing equations satisfy the stipulated boundary conditions [30]. Next, a perturbation analysis will be carried out to describe a linearized version of the governing equations [31]. Lastly, a normal mode analysis will be carried out to describe the vibrational mode at which the occurrence of convective instability is most likely within the reservoir of interest [32].

i) *Steady State Solution*: At steady state, all time derivatives within the governing equations will be zero and all derivatives of the stream function will be zero (since $u_{x(s)} = u_{z(s)} = 0$).

$$\frac{\partial \boldsymbol{\psi}_s}{\partial \boldsymbol{x}} = 0 \tag{18}$$

$$\frac{\partial \boldsymbol{\psi}_s}{\partial \boldsymbol{z}} = 0 \tag{19}$$

Additionally, according to the boundary conditions of the described model, there is no horizontal variation in concentration and temperature at steady state.

$$\frac{\partial \boldsymbol{C}_s}{\partial \boldsymbol{x}} = 0 \tag{20}$$

$$\frac{\partial \boldsymbol{T}_s}{\partial \boldsymbol{z}} = 0 \tag{21}$$

Inserting equations *18*, *19*, *20*, and *21*into equations *15*, *16*and *17*;

$$\frac{d^2 \boldsymbol{C}_s}{d \boldsymbol{z}^2} = 0 \tag{22}$$

$$\frac{d^2 \boldsymbol{T}_s}{d \boldsymbol{z}^2} = 0 \tag{23}$$

Solving equations *22*and *23*;

$$\boldsymbol{C}_s = A\boldsymbol{z} + B \tag{24}$$

$$\boldsymbol{T}_s = C\boldsymbol{z} + D \tag{25}$$

Where A, B, C and D are constants. Recall that $\boldsymbol{z}$ in equations *24*and *25*is actually a non-dimensional variable $\boldsymbol{z} = \frac{z}{H}$. Therefore, the constants in these equations can be quantitatively described by applying the existing boundary conditions of the model; i.e. at $\boldsymbol{z} = 0$ ($z = 0$), $C = 1$, $T = 0$ and at $\boldsymbol{z} = 1$ ($z = H$), $C = 0$, $T = 1$. Hence, at steady state,

$$\boldsymbol{C}_s = 1 - \boldsymbol{z} \tag{26}$$

$$\boldsymbol{T}_s = \boldsymbol{z} \tag{27}$$

Evidently, the governing equations satisfy the stipulated boundary conditions since at $\boldsymbol{z} = 0$, $\boldsymbol{C}_s = 1$ and $\boldsymbol{T}_s = 0$.

ii) *Perturbation Analysis*: To do this, there will be an introduction of small perturbations of the order of ϵ (perturbation parameter, where $\epsilon <<<< 1$) to the system variable such that;

$$\boldsymbol{\psi} = \boldsymbol{\psi}_s + \epsilon \boldsymbol{\psi}' \tag{28}$$

$$\boldsymbol{C} = \boldsymbol{C}_s + \epsilon \boldsymbol{C}' \tag{29}$$

$$\boldsymbol{T} = \boldsymbol{T}_s + \epsilon \boldsymbol{T}' \tag{30}$$

Where the prime (') indicates the perturbed system variables. Applying the steady state solutions while inserting equations *28, 29* and *30* into equations *15, 16* and *17* and neglecting terms of $O(\epsilon^2)$, dropping the 'ϵ' notations;

$$\frac{\partial^2 \boldsymbol{\psi}'}{\partial \boldsymbol{x}^2} + \vartheta \frac{\partial^2 \boldsymbol{\psi}'}{\partial \boldsymbol{z}^2} = Ra_S \frac{\partial \boldsymbol{C}'}{\partial \boldsymbol{x}} - Ra_T \frac{\partial \boldsymbol{T}'}{\partial \boldsymbol{z}} \tag{31}$$

$$\frac{\partial \boldsymbol{C}'}{\partial \boldsymbol{t}} - \frac{\partial \boldsymbol{\psi}'}{\partial \boldsymbol{z}} = \frac{\partial^2 \boldsymbol{C}'}{\partial \boldsymbol{x}^2} + \frac{\partial^2 \boldsymbol{C}'}{\partial \boldsymbol{z}^2} \quad (32)$$

$$\frac{\partial \boldsymbol{T}'}{\partial \boldsymbol{t}} + \frac{\partial \boldsymbol{\psi}'}{\partial \boldsymbol{z}} = \frac{1}{Pr}\left[\frac{\partial^2 \boldsymbol{T}'}{\partial \boldsymbol{x}^2} + \frac{\partial^2 \boldsymbol{T}'}{\partial \boldsymbol{z}^2}\right] \quad (33)$$

Equations *31*, *32*and *33*are the linearized form of the governing equations.

iii) *Normal Mode Analysis*: The functional form of the variation of the fluid mechanical variables in space and time is exactly the same for the functional form of the imposed disturbance, which is a quality of only linear problems [33, 34]. Consequently, the imposed disturbance and its manifestation on the fluid mechanical variables is in exactly the same frequency for the linearized governing equations [35].

Hence, assuming a normal mode for the disturbance in terms of some periodic disturbance in the horizontal direction, constrained in the vertical direction, since convective motion is assumed to exhibit horizontal periodicity during normal mode analysis [36, 37]

$$\boldsymbol{\psi}'(x,z,t) = \tilde{\boldsymbol{\psi}} Sin(n\pi z) e^{i\alpha x + \sigma t} \quad (34)$$

$$\boldsymbol{C}'(x,z,t) = \tilde{\boldsymbol{C}} Sin(n\pi z) e^{i\alpha x + \sigma t} \quad (35)$$

$$\boldsymbol{T}'(x,z,t) = \tilde{\boldsymbol{T}} Sin(n\pi z) e^{i\alpha x + \sigma t} \quad (36)$$

Where;

$\alpha =$ Spatial frequency in the horizontal plane

$\sigma =$ Growth rate

$n =$ Number of modes $(1, 2, 3, \ldots\ldots\ldots\ldots N)$

$i = \sqrt{-1}$

Inserting equations *34*, *35*and *36*into the linearized form of the governing equations;

$$[\alpha^2 + \vartheta n^2\pi^2]\tilde{\boldsymbol{\psi}} + i\alpha Ra_S \tilde{\boldsymbol{C}} - i\alpha Ra_T \tilde{\boldsymbol{T}} = 0 \quad (37)$$

$$i\alpha\tilde{\boldsymbol{\psi}} - [\sigma + \alpha^2 + n^2\pi^2]\tilde{\boldsymbol{C}} = 0 \quad (38)$$

$$i\alpha\phi Pr\tilde{\boldsymbol{\psi}} + [\sigma Pr + \alpha^2 + n^2\pi^2]\tilde{\boldsymbol{T}} = 0 \quad (39)$$

From equation *38*,

$$\tilde{\boldsymbol{C}} = \frac{i\alpha}{\sigma + \alpha^2 + n^2\pi^2}\tilde{\boldsymbol{\psi}} \quad (40)$$

From equation *39*,

$$\tilde{\boldsymbol{T}} = \frac{-i\alpha\phi Pr}{\sigma Pr + \alpha^2 + n^2\pi^2}\tilde{\boldsymbol{\psi}} \quad (41)$$

Inserting equations *40*and *41*into equation *37*;

$$\left([\alpha^2 + \vartheta n^2\pi^2] - \left[\frac{\alpha^2 Ra_S}{\sigma + \alpha^2 + n^2\pi^2}\right] - \left[\frac{\alpha^2\phi Pr Ra_T}{\sigma Pr + \alpha^2 + n^2\pi^2}\right]\right)\tilde{\boldsymbol{\psi}} = 0 \quad (42)$$

Using WOLFRAM Mathematica software to seek for the solution of equation *42*,noting that $\tilde{\boldsymbol{\psi}} \neq 0$, for an expression for the thermal Rayleigh number;

$$Ra_T = \frac{(\sigma Pr + \alpha^2 + n^2\pi^2)([\alpha^2 + \vartheta n^2\pi^2][\sigma + \alpha^2 + n^2\pi^2] - \alpha^2 Ra_S)}{(\sigma + \alpha^2 + n^2\pi^2)\alpha^2\phi Pr} \quad (43)$$

Since for instability to be initiated and sustained the perturbation introduced in the system as a result of fluctuations in system variables, as defined by the growth rate σ of the disturbance, must not die off. This is only achievable when $\sigma \geq 0$. In other words, stationary convection would only be initiated if the minimum value of the growth rate, σ_{min}, is zero [5, 6]. Additionally, the minimum node at which stationary convection will be initiated is when $n = 1$[38].

Evaluating equation *43*at $\sigma = 0$ and $n = 1$ for the onset of stationary convection,

$$Ra_T^{st} = \frac{(\alpha^2 + \vartheta\pi^2)(\alpha^2 + \pi^2) - \alpha^2 Ra_S}{\alpha^2\phi Pr} \quad (44)$$

Various authors [5, 19, 39] have shown that Ra_T^{st} has a critical value when $\alpha_{crit} = \pi$. Hence, evaluating equation *44* at $\alpha = a_{crit}$, the condition then becomes that instability will set in if,

$$Ra_T^{st} > Ra_{T,crit}^{st} = \frac{2\pi^2(1 + \vartheta) - Ra_{S,crit}}{\phi Pr} \quad (45)$$

For $\vartheta = \phi = Pr = 1$;

$$Ra_{T,crit}^{st} = 4\pi^2 - Ra_{S,crit} \quad (46)$$

This is similar to the results obtained by Wang and Tan [37], Phillips [38] and Israel-Cookey and Omubo-Pepple [40] for an isotropic porous media.

There will be a further investigation of how stationary thermal Rayleigh number, Ra_T^{st}, affects the onset of convective instability. This will be done by quantitatively describing how all the physical variables that are used in defining Ra_T^{st} (as can be seen in equation *44*) influences the onset of convective instability for different wave numbers, α. The various other parameters used for this purpose is shown in Table *1*.

Table 1: Fluid Properties [41]

Parameters	**Numerical Values**
Viscosity, μ	$5 \times 10^{-4}\ Pa\ s$
Brine density, ρ_o	$994.56\ kgm^{-3}$
Density change due to CO_2 dissolution, $\Delta\rho_c$	$10.45\ kgm^{-3}$
Diffusivity, D	$2 \times 10^{-9} m^2 s^{-1}$
Acceleration due to gravity, g	$9.80 ms^{-2}$

III. RESULTS

After defining a relationship between the stationary thermal Rayleigh number, wave number and other fluid mechanical variables of the modelled system, there arose a need to describe how all of these fluid mechanical variables influenced the onset of convective instability within the study area. This need was met by obtaining the value of the stationary Rayleigh number for different values of wave number at different values of fluid mechanical variables and then creating a 2D plot of the thermal Rayleigh number against the wave numbers.

To begin with, the stationary thermal Rayleigh number was plotted against wave number for different values of permeability anisotropy ratio to investigate how permeability anisotropy ratio affects the onset of convective instability. The estimates of the different values of stationary Rayleigh number for different values of permeability anisotropy ratio and its accompanying plot is shown in Table 2 and Figure 2.

Table 2:Measure of Stationary Thermal Rayleigh Number for Different Wavenumbers at Different Values of Permeability Anisotropy Ratio

α	$Ra_T(\vartheta)$					
	0.5	**0.6**	**0.7**	**0.8**	**0.9**	**1**
1	−1743.76	−1736.47	−1729.17	−1721.87	−1714.57	−1707.27
2	−1766.57	−1764.24	−1761.92	−1759.59	−1757.26	−1754.93
3	−1767.77	−1766.36	−1764.96	−1763.55	−1762.14	−1760.73
4	−1764.62	−1763.53	−1762.45	−1761.36	−1760.28	−1759.19
5	−1759.24	−1758.31	−1757.37	−1756.43	−1755.5	−1754.56
6	−1752.17	−1751.31	−1750.45	−1749.6	−1748.74	−1747.89
7	−1743.57	−1742.76	−1741.95	−1741.15	−1730.42	−1729.65
8	−1733.52	−1732.75	−1731.97	−1731.2	−1730.42	−1729.65
9	−1722.06	−1721.31	−1720.56	−1719.8	−1719.05	−1718.3
10	−1709.22	−1708.48	−1707.74	−1707	−1706.27	−1705.53

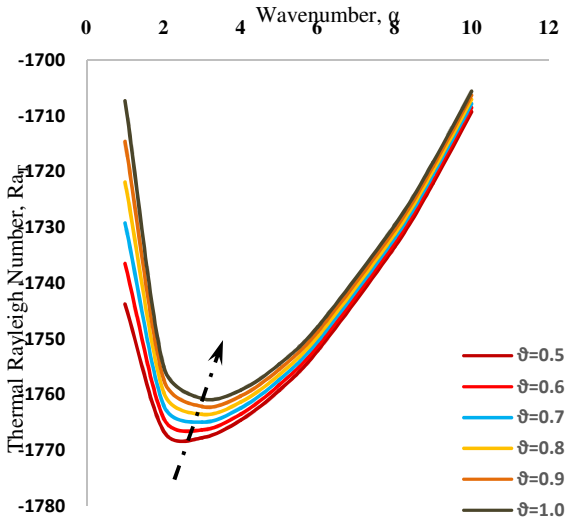

Fig. 2: A plot of stationary thermal Rayleigh Number against wave number for different values of permeability anisotropy ratio

Furthermore, the stationary thermal Rayleigh number was plotted against wave number for different values of Prandtl number to investigate how permeability anisotropy ratio affects the onset of convective instability. The estimates of the different values of stationary Rayleigh number for different values of Prandtl number and its accompanying plot is shown in Table 3 and Figure 3.

Table 3:Measure of Stationary Thermal Rayleigh Number for Different Wavenumbers at Different Values of Prandtl Number

α	$Ra_T(\boldsymbol{Pr})$					
	2	**4**	**6**	**8**	**10**	**12**
1	−6039.31	−3019.66	−2013.1	−1509.83	−1207.86	−1006.55
2	−6162.63	−3081.32	−2054.21	−1540.66	−1232.53	−1027.11
3	−6174.88	−3087.44	−2058.29	−1543.72	−1234.98	−1029.15
4	−6166.67	−3083.34	−2055.56	−1541.67	−1233.33	−1027.78
5	−6149.16	−3074.58	−2049.72	−1537.29	−1229.83	−1024.86
6	−6125.09	−3062.55	−2041.7	−1531.27	−1225.02	−1020.85
7	−6095.42	−3047.71	−2031.81	−1523.86	−1219.08	−1015.9
8	−6060.54	−3030.27	−2020.18	−1515.14	−1212.11	−1010.09
9	−6020.64	−3010.32	−2006.88	−1505.16	−1204.13	−1003.44
10	−5975.81	−2987.9	−1991.94	−1493.95	−1195.16	−995.968

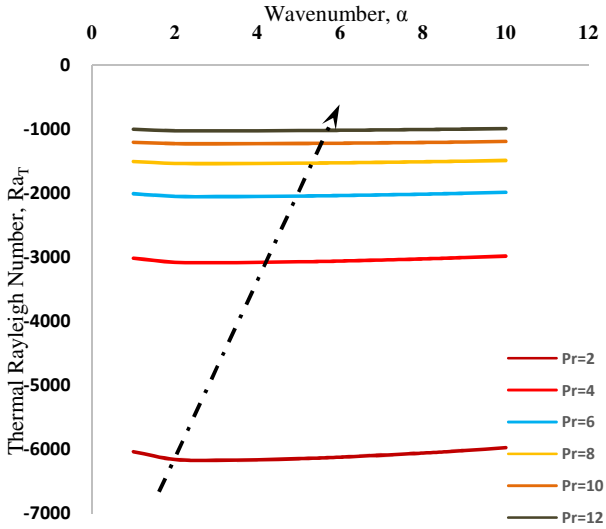

Fig. 3:A plot of stationary thermal Rayleigh Number against wave number for different values of Prandtl Number

Additionally, the stationary thermal Rayleigh number was plotted against wave number for different values of porosity to investigate how permeability anisotropy ratio affects the onset of convective instability. The estimates of the different values of stationary Rayleigh number for different values of porosity and its accompanying plot is shown in Table 4 and Figure 4.

Table 4:Measure of Stationary Thermal Rayleigh Number for Different Wavenumbers at Different Values of Porosity

α	$Ra_T(\boldsymbol{\phi})$					
	0.12	**0.15**	**0.18**	**0.21**	**0.24**	**0.27**
1	−3063.42	−2450.74	−2042.28	−1750.53	−1531.71	−1361.52
2	−3125.97	−2500.78	−2083.98	−1786.27	−1562.99	−1389.32
3	−3132.19	−2505.75	−2088.13	−1789.82	−1566.09	−1392.08
4	−3128.02	−2502.42	−2085.35	−1787.44	−1564.01	−1390.23
5	−3119.14	−2495.31	−2079.43	−1782.36	−1559.57	−1386.28
6	−3106.93	−2485.55	−2071.29	−1775.39	−1553.47	−1380.86
7	−3091.88	−2473.51	−2061.25	−1766.79	−1545.94	−1374.17
8	−3074.19	−2459.35	−2049.46	−1756.68	−1537.09	−1366.31
9	−3053.95	−2443.16	−2035.96	−1745.11	−1526.97	−1357.31
10	−3031.21	−2424.96	−2020.8	−1732.12	−1515.6	−1347.2

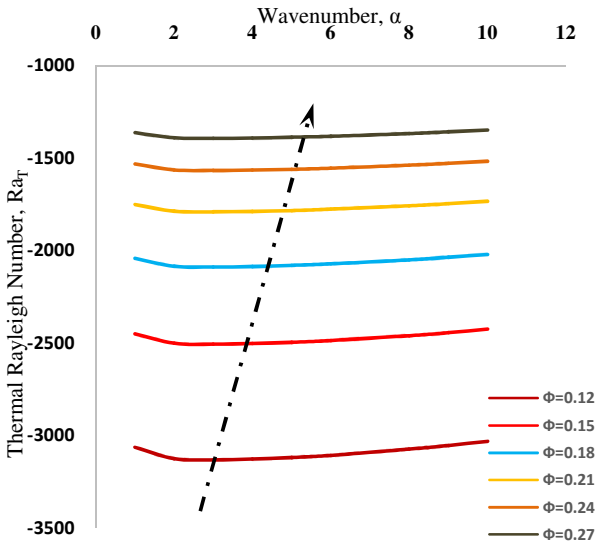

Fig. 4: A plot of stationary thermal Rayleigh number against wave number for different values of Porosity

Lastly, the stationary thermal Rayleigh number was plotted against wave number for different values of permeability anisotropy ratio to investigate how permeability anisotropy ratio affects the onset of convective instability. The estimates of the different values of stationary Rayleigh number for different values of permeability anisotropy ratio and its accompanying plot is shown in Table 5 and Figure 5.

Table 5:Measure of Stationary Thermal Rayleigh Number for Different Wavenumbers at Different Values of Solutal Rayleigh Number

α	$Ra_T(\boldsymbol{Ra_S})$					
	2667.73	**2816.25**	**2964.77**	**3113.29**	**3261.80**	**3410.32**
1	−1778.06	−1880.55	−1983.05	−2085.55	−2188.04	−2290.54
2	−1813.80	−1916.30	−2018.79	−2121.29	−2223.79	−2326.28
3	−1817.35	−1919.85	−2022.35	−2124.84	−2227.34	−2329.83
4	−1814.97	−1917.47	−2019.97	−2122.46	−2224.96	−2327.45
5	−1809.90	−1912.39	−2014.89	−2117.39	−2219.88	−2322.38
6	−1802.92	−1905.42	−2007.91	−2110.41	−2212.91	−2315.40
7	−1794.32	−1896.82	−1999.31	−2101.81	−2204.31	−2306.80
8	−1784.21	−1886.71	−1989.20	−2091.70	−2194.20	−2296.69
9	−1772.64	−1875.14	−1977.64	−2080.13	−2182.63	−2285.12
10	−1759.65	−1862.15	−1964.64	−2067.14	−2169.63	−2272.13

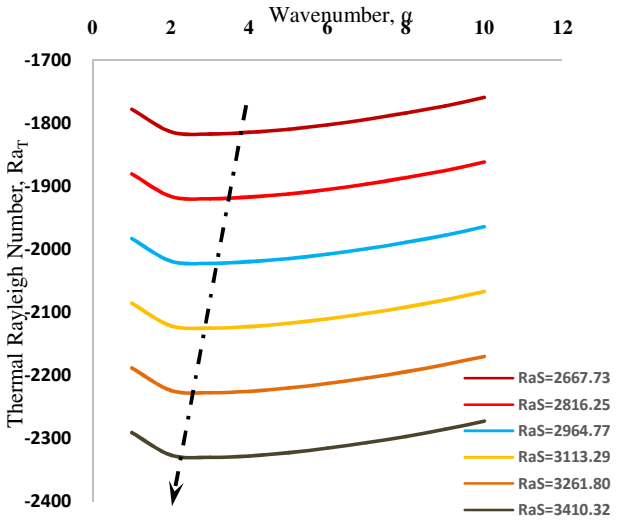

Fig. 5:A plot of stationary thermal Rayleigh number against wave number for different values of Solutal Rayleigh Number

IV. DISCUSSION

What happens after the supercritical CO_2 has been successfully sequestered? Considering the risk of further environmental degradation, this question is of uttermost importance. Various authors [42, 43, 44] have suggested that different trapping mechanisms begin to take effect after sequestration relative to physical, chemical and hydrodynamic conditions within the geologic storage unit. These mechanisms are said to be of four categories; residual trapping, hydrodynamic trapping, mineral trapping and solubility trapping. This study is however focused on the mechanism of solubility trapping of the sequestered CO_2 initiated by density-driven convective mixing as a result of solutal and thermal

fields contributing to the buoyancy field in opposite directions, with the solutal field as the destabilizing field and the thermal field as the stabilizing field.

To investigate how certain reservoir variables influence convective mixing within the Niger Delta, cases for varying permeability anisotropy ratio, Prandtl number, porosity and solutal Rayleigh number were analysed relative to neural stability curves of stationary thermal Rayleigh number against wavenumber.

Chan Kim and Kyun Choi [23] had shown that the minimum of such curves is indicative of the critical time at which convective instability is initiated. In other words, in these kinds of comparative analysis, the curve with the *least* minimum suggest an earlier onset time. This is only valid if the Rayleigh number has a destabilizing effect, i.e. for positive Rayleigh numbers. In this study however since the thermal field is stabilizing, the estimated thermal Rayleigh numbers were negative. Hence, the neural stability curve with the *most* minimum will be indicative of an earlier onset of convective instability.

A. Effect of Permeability Anisotropy

By definition, the permeability anisotropy ratio is a dimensionless variable that provides a quantitative measure of the vertical permeability relative to the horizontal permeability within a heterogenous porous media [45]. Considering that the reservoirs within the Niger Delta are predominantly heterogenous, there arose a need within this study to investigate to what extent does permeability anisotropy affects the onset of convective mixing. To do this, a neural stability curve of stationary thermal Rayleigh number (as described by equation *42*) and wave numbers $(1-10)$ was analysed for different values of permeability anisotropy ratio, ranging from 0.5 to 1.0. Other variables included in the analysis were average porosity value for a typical Niger Delta Reservoir (taken to be 0.21 according to Davies et al. [46]), a solutal Rayleigh number of 2637.84 (estimated for a typical Niger Delta reservoir according to Davies et al. [47] with a height of $20m$, according to the mathematical description of solutal Rayleigh number from equation *15*) and a Prandtl number of 7, suggestive of an average Prandtl number of water [48, 49]. The results obtained are shown in Table *2*.

The resulting neural stability curve, Figure *2*, shows that the onset of convective mixing is hastened with increasing permeability anisotropy ratio. This is similar to results obtained by other researchers [6, 13, 50]. This is quite expected as increasing permeability anisotropy ratio is indicative of an enhanced vertical flow of fluid, which is favorable to more solute diffusion in the vertical direction, enhancing the onset of instability.

B. Effect of Prandtl number

By definition, Prandtl number is said to be a dimensionless variable that provides a quantitative measure of the momentum diffusion relative to thermal diffusion within a body of fluid [51]. Considering that the convective mixing within this study is influenced by both solutal and thermal fields, there will be a need to investigate how varying momentum and thermal diffusivities, in term of Prandtl number, will influence the onset of convective instability. To this end, a neural stability curve of stationary thermal Rayleigh number (as described by equation *42*) and wave numbers $(1-10)$ was analysed for different values of Prandtl number, ranging from 2 to 12, which falls within the range of the Prandtl number for water according to The Engineering Toolbox [52]. Other variables included in the analysis were average porosity and solutal Rayleigh number as described previously and a permeability anisotropy ratio of 0.75, estimated as the average of the range of values used in the previous analysis. The results obtained are shown in Table *3*.

The resulting neural stability curve, Figure *3*, shows that the onset of convective mixing is also hastened with increasing Prandtl number, which is in agreement with results obtained by other researchers [17, 53]. This shows that increase in Prandtl number (indicative of increasing momentum diffusivity relative to thermal diffusivity, represents increased rate of solute transport relative to thermal transport) enhances the destabilizing effect within the fluid, hence enhancing the onset of convective instability.

Further analysis of the neural stability curve, Figure *3*, reveals that the change in critical time at which convection is initiated is smaller for equal magnitude of change in higher Prandtl number relative to lower Prandtl number. This could be suggestive of the fact that at higher values of Prandtl number the fluid has become so saturated by momentum diffusion that any change in Prandtl number will cause smaller destabilizing effect relative to changes at lower values of Prandtl number.

C. Effect of Reservoir Porosity

Porosity have often been defined as how much pore volume is available in the rock matrix relative to the bulk volume of the rock [46, 54]. It is indicative of how much fluid a porous media is capable of holding. The quantitative description of stationary thermal Rayleigh number in this study, as seen in equation *42*, shows that the porosity of the formation is crucial in the onset of convective mixing. Besides, according to Wangen [55], reactive fluids have the tendency to alter the matrix of the storing geologic reservoir, thereby influencing the onset of instability. So, the question becomes 'how does changing porosity influence the onset of convective mixing?'.

To answer this question, a neural stability curve of stationary thermal Rayleigh number (as described by equation *42*) and wave numbers $(1-10)$ was analysed for different values of porosity, taken as the range of typical values of porosities in the Niger Delta according to Davies et al. [46]. Other variables included in this analysis were a Prandtl number of 7 (suggestive of an average Prandtl number of water according to Cioni et al. [49] and Rapp [48]), a solutal Rayleigh number as described previously and a permeability anisotropy ratio of 0.75, estimated as the average of the range of values used in the previous analysis. The results obtained are shown in Table *4*.

The resulting neural stability curve, Figure *4*, shows that the onset of convective mixing is also hastened with increasing porosity, assuming the reservoir is sufficiently permeably of course. This result is not entirely surprising as various authors [55, 56, 57] have acknowledged the importance of a porous media to the onset convective mixing.

However, upon further analysis of the obtained results as seen in Figure *4*, the interesting aspect of this result is the degree of change of the critical onset time with equal magnitudes of increasing porosity. It becomes evident that at equal magnitude of change in higher values of porosity relative to lower values of porosity, as observed for changing Prandtl number, the change in critical onset time becomes relatively smaller. This could just imply that at higher values of porosity for a permeable reservoir unit, the destabilizing regime undergoes relatively smaller changes for changes in porosity as the fluid could have been sufficiently saturated with the destabilizing agent. Therefore, it can therefore be sufficed that as the porosity becomes infinitely large, the change in the critical onset time for convective mixing becomes, relatively, infinitely small.

D. Effect of Solutal Rayleigh Number: Rayleigh number (solutal or thermal), is said to be a dimensionless number that aids in predicting the onset of convective instability [21, 22]. In this study, considering that critical values of thermal Rayleigh number has been employed in defining the onset of convective instability and that solutal Rayleigh number is shown as an influencing variable on the thermal Rayleigh number, as seen in equation *42*, the question then becomes 'how is convective mixing influenced by solutal Rayleigh number?'.

To answer this question, a neural stability curve of stationary thermal Rayleigh number (as described by equation 3.50) and wave numbers $(1 - 10)$ was analysed for different values of solutal Rayleigh number. The different values of solutal Rayleigh number was obtained for a range of values of permeability for typical sandstone reservoirs in the Niger Delta according to Davies et al. [47], in meter-square, as described previously. Other variables included in this analysis were a Prandtl number of 7 (suggestive of an average Prandtl number of water according to Cioni et al. [49] and Rapp [48]), average porosity value (as previously described) and a permeability anisotropy ratio of 0.75, estimated as the average of the range of values used in previous analysis. The results obtained are shown in Table *5*.

The resulting neural stability curve, Figure *5*, shows that the onset of convective mixing is delayed with increasing solutal Rayleigh number. This result is similar to results obtained by Okeke et al. [58]. This result, of course, is expected since Rayleigh [20] himself had shown that, in the destabilizing regime, the smaller the critical value of the Rayleigh number, the earlier the onset of convective instability. In other words, as the critical value gets larger, onset time gets relatively later.

V. CONCLUSION & RECOMMENDATION

A. Conclusion

Looking to investigate the influence of geothermal reservoir variables in the Niger Delta on the onset of convective instabilityduring solubility trapping of sequestered CO_2, linear stability analysis, based on the principle of exchange of instabilities, of the hydrodynamic governing equations was carried out. This led to a mathematical relationship that showed that the onset of instability after CO_2 sequestration, as defined by thermal Rayleigh number and perturbation wave number, is influenced by permeability anisotropy ratio, Prandtl number, porosity and solutal Rayleigh number. Analysing series of 2D plots of thermal Rayleigh number and perturbation wave number relative to reservoir variables, varying the reservoir variable under investigation while keeping the other reservoir variables constant, showed that;

i. The onset of convective instability is hastened relative to increasing permeability anisotropy ratio, Prandtl number and porosity
ii. The onset of convective instability is delayed relative to increasing solutal Rayleigh number.
iii. Therefore, it can be said that reservoir variables like permeability anisotropy ratio, Prandtl number, porosity and solutal thermal number play major roles in solubility trapping of sequestered CO_2 in the Niger Delta.

B. Recommendation

To account for the progress of convective mixing of sequestered CO_2 after its onset, there would be a need to carry out proper numerical simulations of the governing equations, with the accompanying boundary conditions, to properly estimate the exact time for the onset and progress of convective mixing.

ACKNOWLEDGEMENT

The authors are grateful to Mr. Ene Donald of the Information and Communication Technology Centre of the Rivers State University, Port Harcourt, for his assistance during the period of this research. Also, we will like to thank Mrs. Blessing O. Davies for her insight and encouragement while this research lasted.

REFERENCES

1. Huppert, H.E. and J.A. Neufeld, The fluid mechanics of carbon dioxide sequestration. Annual Review of Fluid Mechanics, 2014. 46: p. 255-272.
2. Hidalgo, J.J. and J. Carrera, Effect of dispersion on the onset of convection during CO_2 sequestration. Journal of Fluid Mechanics, 2009. 640: p. 441-452.
3. Emami-Meybodi, H., H. Hassanzadeh, C.P. Green, and J. Ennis-King, Convective dissolution of CO_2 in saline aquifers: Progress in modeling and experiments. International Journal of Greenhouse Gas Control, 2015. 40: p. 238-266.
4. Riaz, A. and Y. Cinar, Carbon dioxide sequestration in saline formations: Part I—Review of the modeling of solubility trapping. Journal of Petroleum Science Engineering, 2014. 124: p. 367-380.
5. Pritchard, D. and C.N. Richardson, The effect of temperature-dependent solubility on the onset of thermosolutal convection in a horizontal porous layer. Journal of Fluid Mechanics, 2007. 571: p. 59-95.

6. Bhadauria, B., Double-diffusive convection in a saturated anisotropic porous layer with internal heat source. Transport in porous media, 2012. 92(2): p. 299-320.
7. Thomas, C., S. Dehaeck, and A. De Wit, Convective dissolution of CO_2 in water and salt solutions. International Journal of Greenhouse Gas Control, 2018. 72: p. 105-116.
8. Ennis-King, J.P. and L. Paterson, Role of convective mixing in the long-term storage of carbon dioxide in deep saline formations. Society of Petroleum Engineers Journal, 2005. 10(03): p. 349-356.
9. Hidalgo, J.J., J. Fe, L. Cueto-Felgueroso, and R. Juanes, Scaling of convective mixing in porous media. Physical review letters, 2012. 109(26): p. 264503.
10. Emami-Meybodi, H., Stability analysis of dissolution-driven convection in porous media. Physics of Fluids, 2017. 29(1): p. 014102.
11. Horton, C. and F. Rogers Jr, Convection currents in a porous medium. Journal of Applied Physics, 1945. 16(6): p. 367-370.
12. Lapwood, E. Convection of a fluid in a porous medium. in Mathematical Proceedings of the Cambridge Philosophical Society. 1948. Cambridge University Press.
13. Farajzadeh, R., F.F. Zinati, P. Zitha, and J. Bruining. Density-driven Natural Convection in Dual Layered and Anisotropic Porous Media with Application for CO_2 Injection Project. in ECMOR XI-11th European Conference on the Mathematics of Oil Recovery. 2008. European Association of Geoscientists & Engineers.
14. Hirata, S., B. Goyeau, and D. Gobin, Stability of thermosolutal natural convection in superposed fluid and porous layers. Transport in porous media, 2009. 78(3): p. 525-536.
15. Li, Q., Coupled reactive transport model for heat and density driven flow in CO_2 storage in saline aquifers. Journal of Hazardous, Toxic, Radioactive Waste, 2011. 15(4): p. 251-258.
16. Akand, W.I., A.R.S. Muhammed, and S.C. Eric, Numerical investigation of double diffusive natural convection of CO_2 in a brine saturated geothermal reservoir. Elsevier, 2013. 48: p. 101-111.
17. Negara, A., A. Salama, and S. Sun. Density-Driven Flow Simulation in Anisotropic Porous Media: Application to CO_2 Geological Sequestration. in SPE Saudi Arabia Section Technical Symposium and Exhibition. 2014. Society of Petroleum Engineers.
18. De Paoli, M., F. Zonta, and A. Soldati, Influence of anisotropic permeability on convection in porous media: Implications for geological CO_2 sequestration. Physics of fluids, 2016. 28(5): p. 056601-056619.
19. Israel-Cookey, C., E. Amos, and L. Ebiwareme, Soret and magnetic field effects on thermosolutal convection in a porous medium with concentration based internal heat source. American Journal of Fluid Dynamics, 2018. 8(1): p. 1-6.
20. Rayleigh, L., LIX. On convection currents in a horizontal layer of fluid, when the higher temperature is on the underside. The London, Edinburgh, Dublin Philosophical Magazine Journal of Science, 1916. 32(192): p. 529-546.
21. Wang, S. and W. Tan, Stability analysis of soret-driven double-diffusive convection of Maxwell fluid in a porous medium. International Journal of Heat Fluid Flow, 2011. 32(1): p. 88-94.
22. Prasad, A. and C.T. Simmons, Unstable density ‐ driven flow in heterogeneous porous media: A stochastic study of the Elder [1967b] "short heater" problem. Water Resources Research, 2003. 39(1): p. SBH 4-1-SBH 4-21.
23. Chan Kim, M. and C. Kyun Choi, Linear stability analysis on the onset of buoyancy-driven convection in liquid-saturated porous medium. Physics of Fluids, 2012. 24(4): p. 044102.
24. Ogagarue, D., J. Ebeniro, and C. Ehirim, Velocity anisotropy in the Niger Delta Basin: A case study of prestack time imaging with isotropic and anisotropic velocity models. Archives of Physics Research, 2010. 1(2): p. 50-57.
25. Okorie, I.P., J.O. Ebeniro, and C.N. Ehirim, Anisotropy and Empirical Relations for the Estimation of Anisotropy Parameters in Niger Delta Depobelts. International Journal of Geosciences, 2016. 7(3): p. 345-352.
26. Ennis-King, J., I. Preston, and L. Paterson, Onset of convection in anisotropic porous media subject to a rapid change in boundary conditions. Physics of Fluids, 2005. 17(8): p. 084107.
27. Akand, W.I., K.N.K. Aboulghasem, S. Kamy, and P. Tad, Effects of geochemical reaction on double diffusive natural convection of CO_2 in brine saturated geothermal reservoir. Elsevier, 2014. 63: p. 5357-5377.
28. Akand, W.I., R.L. Hamid, and S. Kamy, Double diffusive natural convection of CO_2 in a brine saturated geothermal reservoir: Study of non-modal growth of perturbations and heterogeneity effects. Elsevier, 2014. 51: p. 325-336.
29. Rylov, Y.A., Hydrodynamic equations for incompressible inviscid fluid in terms of generalized stream function. International Journal of Mathematics and Mathematical Sciences, 2004. 2004(11): p. 541-570.
30. Li, Y., Steady-state solution for a general Schnakenberg model. Nonlinear Analysis: Real World Applications, 2011. 12(4): p. 1985-1990.
31. Pieringer, J., T. Sattelmayer, and F. Fassl, Simulation of combustion instabilities in liquid rocket engines with acoustic perturbation equations. Journal of propulsion power, 2009. 25(5): p. 1020-1031.
32. Goldstein, H., C. Poole, and J. Safko, Classical mechanics. 2002, American Association of Physics Teachers.
33. Monin, A.S. and A.M. Yaglom, Statistical fluid mechanics, volume II: mechanics of turbulence. Vol. 2. 2013: Courier Corporation.
34. Majda, A., Compressible fluid flow and systems of conservation laws in several space variables. Vol. 53. 2012: Springer Science & Business Media.
35. Borodulin, V., Y.S. Kachanov, D. Koptsev, and A. Roschektayev, Experimental study of resonant interactions of instability waves in self-similar boundary layer with an adverse pressure gradient: ii. Detuned resonances*. Journal of Turbulence, 2002. 3(62).
36. Tan, W. and T. Masuoka, Stability analysis of a Maxwell fluid in a porous medium heated from below. Physics Letters A, 2007. 360(3): p. 454-460.
37. Wang, S. and W. Tan, Stability analysis of double-diffusive convection of Maxwell fluid in a porous medium heated from below. Physics Letters A, 2008. 372(17): p. 3046-3050.
38. Phillips, O.M., Geological fluid dynamics: sub-surface flow and reactions. 2009: Cambridge University Press.
39. Javaheri, M., J. Abedi, and H. Hassanzadeh, Linear stability analysis of double-diffusive convection in porous media, with application to geological storage of CO_2. Transport in porous media, 2010. 84(2): p. 441-456.
40. Israel-Cookey, C. and V. Omubo-Pepple, Onset of convection of a reacting fluid layer in a porous medium with temperature-dependent heat source. American Journal of Scientific Industrial Research, 2011. 2(6): p. 860-864.
41. Tewes, F. and F. Boury, Formation and Rheological Properties of the Supercritical CO_2– Water Pure Interface. The Journal of Physical Chemistry B, 2005. 109(9): p. 3990-3997.
42. Belhaj, H. and A. Bera, A brief review of mechanisms for carbon dioxide sequestration into aquifer reservoirs. International Journal of Petroleum Engineering, 2017. 3(1): p. 49-66.
43. Zhang, D. and J. Song, Mechanisms for geological carbon sequestration. Procedia IUTAm, 2014. 10(0): p. 319-327.
44. Raza, A., R. Rezaee, C.H. Bing, R. Gholami, M.A. Hamid, and R. Nagarajan, Carbon dioxide storage in subsurface geologic medium: A review on capillary trapping mechanism. Egyptian Journal of Petroleum, 2016. 25(3): p. 367-373.
45. Meyer, R., Anisotropy of sandstone permeability. CREWES Reaserch Report, 2002. 14: p. 1-12.
46. Davies, O.A., D.H. Davies, and P.A. Ngeri, Comparative Analysis of Porosity Estimates in a Sandstone Reservoir: The Niger Delta as Case Study. Journal of Scientific and Engineering Research, 2018. 5(11): p. 102-111.
47. Davies, O.A., C. Israel-Cookey, D.H. Davies, and P.S. Nwiyor, Permeability Modelling of a Sandstone Reservoir in Parts of the Niger Delta. Asian Journal of Applied Science and Technology, 2019. 3(3): p. 73-89.
48. Rapp, B.E., Microfluidics: modeling, mechanics and mathematics. 2016: William Andrew.
49. Cioni, S., S. Ciliberto, and J. Sommeria, Experimental study of high-Rayleigh-number convection in mercury and water. Dynamics of Atmospheres Oceans, 1996. 24(1-4): p. 117-127.
50. Gautam, K. and P. Narayana, On the stability of carbon sequestration in an anisotropic horizontal porous layer with a first-order chemical reaction. Proceedings of the Royal Society A, 2019. 475(2226): p. 20180365.

51. Patience, G.S., Experimental methods in chemical engineering: Preface. The Canadian Journal of Chemical Engineering, 2018. 96(11): p. 2312-2316.
52. The Engineering Toolbox. Water - Prandtl Number. 2020 [cited 2020 May 20th]; Available from: https://www.EngineeringToolBox.com.
53. Bera, P. and A. Khalili, Influence of Prandtl number on stability of mixed convective flow in a vertical channel filled with a porous medium. Physics of Fluids, 2006. 18(12): p. 124103.
54. Guo, B., K. Sun, and A. Ghalambor, Well productivity handbook. 2014: Elsevier.
55. Wangen, M., Stability of reaction-fronts in porous media. Applied Mathematical Modelling, 2013. 37(7): p. 4860-4873.
56. Elenius, M.T. and K. Johannsen, On the time scales of nonlinear instability in miscible displacement porous media flow. Computational Geosciences, 2012. 16(4): p. 901-911.
57. Nield, D. and A. Kuznetsov, Thermal instability in a porous medium layer saturated by a nanofluid. International Journal of Heat Mass Transfer, 2009. 52(25-26): p. 5796-5801.
58. Okeke, I.T., C. Israel-Cookey, E.D. Uko, and M.A. Alabraba, Onset of Rayleigh-Benard Convection in CO_2 Sequestration in the Isotropic Porous Medium within Eastern Niger Delta Region. Asian Journal of Applied Science and Technology, 2019. 3(4): p. 158-178.

